Westerhaus, M., Wyss, M., Yilmaz, R., Zschau, J. (2002): Correlating variations of b values and crustal deformations during the 1990s may have pinpointed the rupture initiation of the Mw = 7.4 Izmit earthquake of 1999 August 17. - Geophysical Journal International, 148, 1, pp. 139—152.

DOI: http://doi.org/10.1046/j.0956-540x.2001.01554.x

Geophys. J. Int. (2002) **148,** 139–152

Correlating variations of *b* values and crustal deformations during the 1990s may have pinpointed the rupture initiation of the $M_w = 7.4$ Izmit earthquake of 1999 August 17

Malte Westerhaus,[1,*] Max Wyss,[2] Rüchan Yilmaz[3] and Jochen Zschau[1]

[1] *GeoForschungsZentrum, Telegrafenberg* A31, 14473 *Potsdam, Germany*
[2] *Geophysical Institute, University of Alaska, Fairbanks,* 99775, *USA*
[3] *Earthquake Research Institute, Ministry of Public Works and Settlement, Ankara, Turkey*

Accepted 2001 July 2. Received 2001 June 29; in original form 2000 July 31

SUMMARY

The *b* value increases from 1.1 along straight segments to 1.7 along a releasing bend of the North Anatolian Fault System between 30.1°E and 30.8°E. The tensional nature of the bend is corroborated by extension rates of 0.3 μstrain yr^{-1} as obtained from Global Positioning System (GPS) data. Fault plane solutions in this area change from abundant right-lateral strike-slip to oblique slip with normal components in the central part of the bend, compatible with the formation of a pull-apart basin. We suggest that this crustal volume is highly fractured, corresponding to a short mean crack length, due to the superposition of horizontal and normal faulting. As a consequence of low normal stress on the existing cracks, frictional sliding is assumed to be the predominant mechanism for the generation of seismic events, resulting in high *b* values. The lowest *b* values ($b \sim 0.8$) in the area investigated are found at the junction between the fault bend and the adjoining segment, which runs through the epicentre of the 1999 Izmit earthquake. At the junction, a localized stress concentration is expected from numerical models of seismicity along geometrical barriers. Thus, the site of lowest *b* has been considered to be the most likely place for a major earthquake, a conclusion that is confirmed by the Izmit earthquake, with epicentre located about 13 km from the anticipated site.

In early 1992, the spatially averaged *b* value started to increase along the central and northwestern parts of the fault bend, and there was a corresponding period of intensified horizontal extension. Since no large earthquake was recorded in 1992, it is assumed that the anomalous extension and the associated change in stress have been caused by aseismic fault creep. In view of the available seismotectonic information, surface displacements due to a slow dislocation at depth were calculated. The GPS data are reasonably explained by a source of normal fault type at a depth of 10 km and equivalent magnitude $M_W = 5.9$. Stress changes at seismogenic depths are calculated under the assumption that an increase in *b* is most likely to be observed along those segments where both deviatoric and mean stress are reduced, while the Coulomb stress change is positive; that is, the fault is brought closer to failure. For right-lateral strike-slip, the stress condition is fulfilled at the sites of the largest *b*-value increase.

The surface rupture of the Izmit earthquake is associated with known fault traces only in the west and in the east of the study area. Along the fault bend, it detaches itself from mapped fault traces and runs through the regions of positive Coulomb stress change caused by the inferred 1992 slow event. Maximum surface slip (5 m) is observed in the immediate vicinity of sites of maximum Coulomb stress change (~ 3 bar), indicating that the 1992 event could have partially unclamped the rupture plane of the subsequent Izmit earthquake. We propose that the strong differences in *b* observed along the complex fault bend can be used to characterize different states of tectonic deformation in space and time.

Key words: *b* values, creep, normal faulting, North Anatolian fault, seismicity, stress distribution.

* Now at: Geodetic Institute, University of Karlsruhe, 76128 Karlsruhe, Germany. E-mail:westerh@gik.uni-karlsruhe.de

INTRODUCTION

The relationship between the seismic b value and the damage evolution of stressed rock volumes is well established by laboratory studies and theoretical models (e.g. Main *et al.* 1992). The b value relates the frequency of occurrence and the magnitude of earthquakes according to the frequency–magnitude distribution (FMD) (Ishimoto & Iida 1939; Gutenberg & Richter 1944):

$$\log_{10} n = a - bM\,, \tag{1}$$

where n is the cumulative number of earthquakes having magnitudes larger or equal to M, and a is a constant. From rock failure tests in the laboratory, Mogi (1962) concluded that b is positively correlated with material heteorogeneity, while Scholz (1968) reported a negative correlation of b with the applied shear stress. Subsequent experiments (e.g. Meredith *et al.* 1990) confirmed both results, although showed that the negative correlation between b and stress holds only for the strain hardening phase. Main (1991) provided a theoretical basis for the laboratory observations, assuming a fractal distribution of crack lengths. His work confirms the dependence of the b value on the number of cracks in a given rock volume, the mean crack length, and the applied stress.

On average, b is near unity for most seismically active regions on Earth (e.g. Frohlich & Davis 1993). However, a detailed mapping of b often reveals significant deviations. High b values are observed in regions of (1) decreased shear stress (Urbancic *et al.* 1992), (2) high slip release on earthquake rupture planes (Wiemer & Katsumata 1999, 1998; Sobiesiak 2000), (3) extensional stress (Frohlich & Davis 1993), (4) high pore pressure (Wyss 1973), and (5) fault creep (Amelung & King 1997). Low b values are associated with major earthquakes (Öncel *et al.* 1996a) and highly stressed asperities (Wiemer & Wyss 1997). On the other hand, high b values are reported from areas of increased geological complexity (Lopez Casado *et al.* 1995) and during volcanic intrusions (Wiemer & McNutt 1997; Wyss *et al.* 1997; Wiemer *et al.* 1998), indicating the importance of heterogeneity.

These observations reveal the potential influence of all components of the stress tensor, and the high spatial variability of b, even on a scale of a few kilometres. In this paper, we focus on the fine structure of b along an overstep of the North Anatolian Fault System, located about 130 km east of Istanbul. The area investigated is a small part of subregion 3 of Öncel *et al.* (1996b), who associated spatial variations of b on a regional scale with along-strike changes in the structural or mechanical properties of the North Anatolian Fault between longitudes 23°E and 45°E. We seek to compare spatial and temporal b-value anomalies on a local scale with other known parameters of the crust, with the aim of gathering evidence for the cause of b-value perturbations and, thus, evaluating the power of b as a tool to monitor small-scale changes in the state of deformation of a given crustal volume.

The area of our detailed b-value investigations encompasses the epicentres of the $M_W = 7.4$ Izmit and $M_W = 7.2$ Düzce earthquakes of 1999 August 17, and 1999 November 12, respectively. The data base, a local seismic catalogue of the years 1985–1995, covers a phase of the seismic cycle near the end of the effectively locked period (see Tse & Rice 1986). Investigations of this catalogue started several years prior to the 1999 earthquakes, and in 1998 we had already identified a site close to the subsequent epicentre of the Izmit earthquake as the most likely location for a major earthquake along this section of the North Anatolian Fault Zone. This claim can be found in an earlier version of the present text that was sent to the German Research Foundation in January 1998 as a supplement to the final report of the Turkish–German Joint Project on Earthquake Research (Zschau 1998; the report can be obtained from the authors). Quotations from the original manuscript (marked by italics in the following text) document the level of our understanding before the Izmit main shock. We do this because we believe that conclusions based on logical and scientific reasoning that have been reached before an upcoming earthquake, and thus are completely without influence from the event, are rare and should be documented.

AREA INVESTIGATED

The North Anatolian Fault (NAF) is an intercontinental dextral strike-slip fault and depicts the boundary between Eurasia in the north and the Anatolian block in the south. Comparable in length and seismicity with the San Andreas Fault in California, it accommodates the westward extrusion of the Anatolian plate caused by the collision of the Arabian and Eurasian plates in Eastern Anatolia (e.g. McKenzie 1972). The cumulative displacement along the fault is commonly estimated as about 40 km in the east and 20–30 km in the west (e.g. Barka 1992). However, displacement rates of 22 ± 3 mm yr^{-1} obtained from GPS data (Straub *et al.* 1997) and recent geological studies indicate that the fault displacement may be up to 60 km (G. W. Michel, personal communication 1996).

East of longitude 32°E, deformation related to the apparent extrusion is localized on a fault zone one to several kilometres wide along most of the trace of the NAF system. West of 32°E, the fault splits into several branches, and deformation is rather distributed (e.g. Michel 1994). A major structural feature in the western part of the fault system is a tensional bend, displacing the main fault by about 25 km to the north (Fig. 1). At about 30.4°E and 30.6°E, the bending trace of the main fault intersects two ENE-striking strands of the NAF system. The junction area is seismically active and characterized by a mixture of earthquake mechanisms (Neugebauer *et al.* 1997). In accordance with the general sense of plate motion, dextral strike-slip on vertical, approximately EW-striking faults is the most common mechanism (Fig. 2). In the northwestern part of the overstep, down slip or oblique slip with a normal component accommodates WSW–ENE extension and the formation of a sedimentary basin. According to Neugebauer *et al.* (1997) this part of the releasing bend fits the concept of an opening pull-apart basin. In the central and southeastern parts of the bend, composite fault plane solutions reveal a change from down slip to normal faulting, and a rotation of the extension axis towards NW–SE. Neugebauer *et al.* (1997) assumes that the transfer of displacement from one fault strand to the other in this part of the fault bend takes place along synthetic strike-slip faults, orientated like Riedel shears (N80°W) with respect to the main fault trace (N105°W). At the centre of the fault bend, all types of earthquake mechanisms are found mixed together. The mean rate of horizontal extension along the fault bend, as obtained from repeated, annual GPS campaigns, amounts to 0.2 μstrain yr^{-1} (Fig. 2). The Izmit and Düzce earthquakes of 1999 August 17 and November 12, respectively, ruptured the northern branches only (Fig. 1).

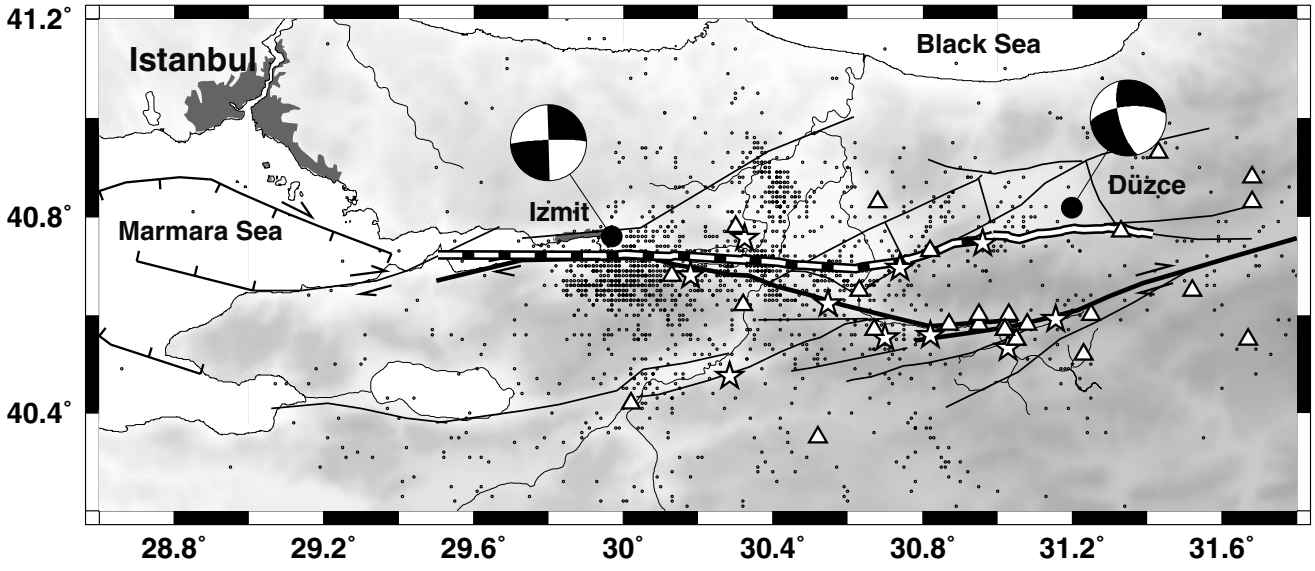

Figure 1. Map of the area investigated by the German–Turkish Project on Earthquake Research along the North Anatolian fault in Turkey, about 150 km east of Istanbul. Dots: epicentres of $M \geq 2$ earthquakes from 1985.0 to 1995.7. Stars: stations of the local seismograph network. Triangles: GPS sites. Fault lines are after Michel (1994) and Barka & Kadinsky-Cade (1988). The trace of the main fault of the North Anatolian Fault System is marked by a solid line, other branches by thin lines. CMT solutions of the two large earthquakes of Izmit (1999 August 17, $M_W = 7.4$) and Düzce (1999 November 12, $M_W = 7.1$) are shown, with the epicentres (large black dots) located at 40.76°N, 29.97°E (Kandilli Observatory) and 40.818°N, 31.198°E (according to the local German–Turkish SABONET; Milkereit, personal communication 1999), respectively. Surface ruptures of the Izmit and Düzce earthquakes are marked by a broken and by a continuous white line, respectively.

Surface breaks are observed for about 170 km, extending from 29.4°E to 31.4°E (Tibi *et al.* 2001). Maximum offsets of up to 5 m are observed in the northwestern part of the bend.

An apparently short recurrence interval of 15–21 years for large ($M \geq 5.5$) earthquakes during the last 100 years was the decisive factor for choosing the area between 32°E and 29°E for the observation cluster of the German–Turkish Earthquake Research Project (Ergünay & Zschau 1989). The interdisciplinary experiment is located around the Mudurnu Valley, along segments of the main fault that were active during the $M = 7.1$ and $M = 7.2$ earthquakes in 1957 and 1967, respectively. Since 1985, seismological, geodetic, gravimetric, magnetic, telluric, isotope-hydrological, meteorological and tilt data have been collected. In this study, we map the *b* value of earthquakes in the vicinity of the fault bend between longitudes 29.8°E and 31.2°E and compare it with the strain rates obtained from annual GPS measurements.

The German–Turkish seismograph network consisted of five stations initially, and was expanded to nine stations between May 1988 and September 1990 (Wyss *et al.* 1995; Neugebauer *et al.* 1997). A tenth station was added in October 1994 as a reaction to an apparent migration of seismic activity towards the west. The seismic catalogue is complete down to a minimum magnitude $M_{min} = 2.0$. In October 1996, the analogue seismic network was replaced by a digital one. Annually repeated GPS measurements have been carried out at 18 monuments

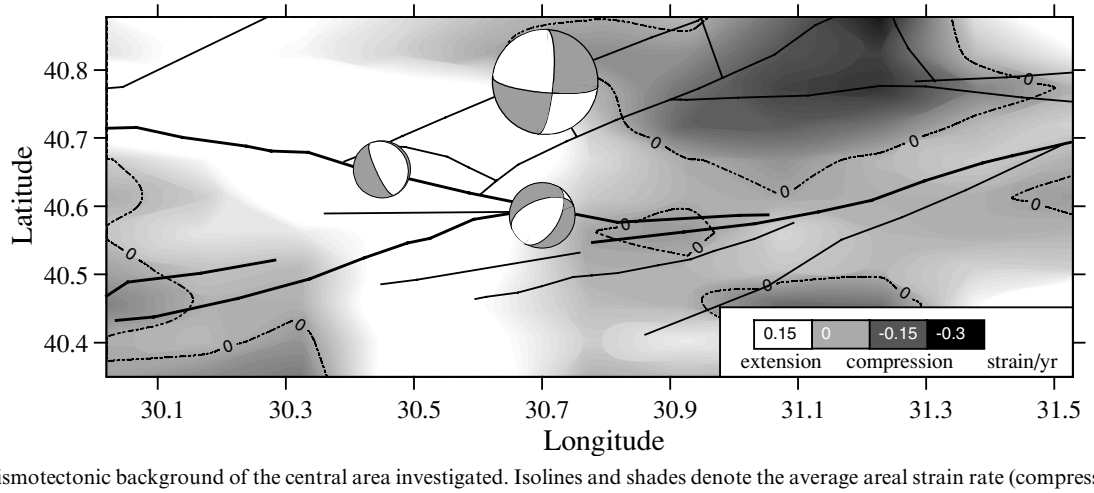

Figure 2. Seismotectonic background of the central area investigated. Isolines and shades denote the average areal strain rate (compression negative) obtained from three GPS campaigns between 1992 and 1995 (data from Altiner 1996). Note that the grey-scale saturates at $+0.15$ μstrain. Extension along the central part of the bend exceeds 0.3 μstrain (*cf.* Fig. 3b). Composite fault plane solutions, obtained from microearthquakes, indicate a spatially varying faulting mechanism (after Neugebauer *et al.* 1997). While the strike-slip mechanism prevails along the northern fault branches, clusters of down slip and normal faulting earthquakes are found in the northwestern and southeastern parts of the releasing bend, respectively.

since September 1990; data with a typical accuracy of 6 mm are available from September 1991 (Altiner 1996). GPS measurements along a 10 km wide north–south profile at about 30.7°E, carried out within the framework of the Marmara polyproject (Straub *et al.* 1997), are not included in the present study because the displacements are given with respect to a different reference station. Comparison of the two data sets is possible in terms of independently derived strains; this was done for the overlapping part of the areas investigated by the two GPS projects.

METHOD

The technique of mapping b values by the computer code ZMAP is explained in detail elsewhere (Wiemer 1996; Wiemer & Benoit 1996; Wiemer & McNutt 1997; Wiemer & Wyss 1997). Very briefly, the b value is estimated at every node of a densely spaced grid, using the n nearest events. The sample volumes have the shape of a cylinder with radius R. Here the number of earthquakes per sample is $n=80$, the nodal separation is 0.02° in map-view and 1 km in cross-sections, and the radius of cylinders beyond which we do not use the b value because it is not based on sufficiently local data is $R_{\max}=25$ km. For comparison, the maps were recompiled with $R=const$ and varying n, with only marginal differences in the spatial b-value pattern. Constant-size volumes ($R_{\text{const}}=15$ km) are also the basis for differential b-value maps, which allow the comparison of the frequency–magnitude distribution at each node for two different periods. The b values presented are calculated by the maximum-likelihood method (Bender 1983), and the general trend of the results is checked by calculating b by least-squares fits (Shi & Bolt 1982). The fits extend from the magnitude of completeness, $M_{\min}$, to the maximum magnitude in the subset of data. Because $M_{\min}$ can vary as a function of depth and location, it is estimated separately for each sample by taking the maximum value of the derivative of the FMD.

For defining anomalies of b values, we estimate the probability, p, that two samples may come from the same population by Utsu's (1992) test:

$$p \approx \exp[-(dA/2) - 2]\,, \tag{2}$$

where

$$dA = -2N\ln N + 2N_1\ln(N_1 + N_2 b_1/b_2) + 2N_2\ln(N_1 b_2/b_1 + N_2) - 2\,,$$

$N=N_1+N_2$, and $N_{1,2}$ represent the number of events in the two samples. We make sure that all anomalies we discuss are significant by imposing two conditions: we do not accept any potential anomaly as significant unless (1) several neighbouring samples show it, and (2) the FMD shows a b value that has a probability of less than 1 per cent of being from the same sample as b of the neighbouring seismicity. Because we are not interested in the accuracy of a single b-value estimate, but in differences between anomalous and background volumes, this test is required to establish significant differences. The individual uncertainties enter indirectly into the estimate of probabilities, but their explicit values are irrelevant and hence not discussed.

The number of earthquakes with $M \geq 2.0$ between January 1985 and August 1995 was 1873. Hour-of-day histograms of the origin times show a maximum around noon for a cluster of earthquakes north of the fault bend at about 30.4°E, 40.8°N, presumably due to a contamination of the catalogue by quarry blasts. Since we do not yet have enough information to separate blast and real events *a priori*, we bordered suspicious regions by polygons and removed that seismicity from the catalogue. This was done in a step-by-step procedure until the histograms revealed an even distribution for all hours of the day, resulting in a reduction of the number of earthquakes to 1277. The density of earthquakes (Fig. 1) is such that the sampling radius is about $R=15\pm10$ km for most nodes if $n=80$. The average b value in the data set is 1.4. We suspect that the magnitude scale used could have been the reason for this relatively high value, an effect sometimes observed in local catalogues. Since we restrict ourselves to the investigation of the relative variations of b, the absolute values are not important.

For comparison of geodetic data with b-value maps, the area covered by 18 GPS stations between longitudes 30.0°E and 31.25°E, and latitudes 40.35°N and 40.85°N has been gridded, and velocity components in NS- and EW-directions resolved at every node (Altiner 1996). To evaluate strain rates, the differences between neighbouring nodes were calculated and divided by the grid distance (6.4 km in a NS-direction, 14.0 km in an EW-direction). This approach is simpler than the procedure used by Altiner (1996), and neglects several effects such as, for example, the curvature of the surface. However, we argue that the shortcomings of the simple approach are of no consequence compared to the uncertainties induced by the uneven distribution of GPS stations over the tectonically complex region. Our results are in agreement with the detailed displacement and strain maps presented by Altiner (1996), and, after resolving for specific faults, are compatible with the results of Straub *et al.* (1997). In comparing geodetic and b-value maps, we focus on first-order spatial phenomena on the scale of tens of kilometres and do not discuss apparent small-scale effects.

RESULTS

A general b-value map calculated from all of the 1277 events in the catalogue gives a first impression of the spatial variability of b (Fig. 3a). With the exception of a bright spot beyond the western margin of the fault bend, normal to moderate b values (1–1.5) prevail in the west of the area investigated. Within the bend, b values are generally higher; extreme values of 2 and above are found in the central area north of the two fault junctions. Towards the northeast b seems to decrease again. This undifferentiated map is a mixture of spatial and temporal features of b.

During the first five years covered by the catalogue (January 1985 to April 1990, Fig. 3b), provinces of high b values are observed east of 30.25°E, and normal values west of 30.25°E. The situation changes drastically for the second half of the catalogue (April 1990 to August 1995, Fig. 3c). An anomaly of high b values north of the fault junctions now appears, and another region of b values above 2 emerges along the western margin of the fault bend within a region where previous b values (Fig. 3b) were low. A plot of b as a function of time, evaluated for a rectangular area bounded by longitudes 30.05°E and 30.50°E, shows a sudden increase of the b value by +0.8 in 1992 (Fig. 4a). Farther to the east (30.6°E to 31.25°E), an opposite trend towards lower b values is indicated (Fig. 4b).

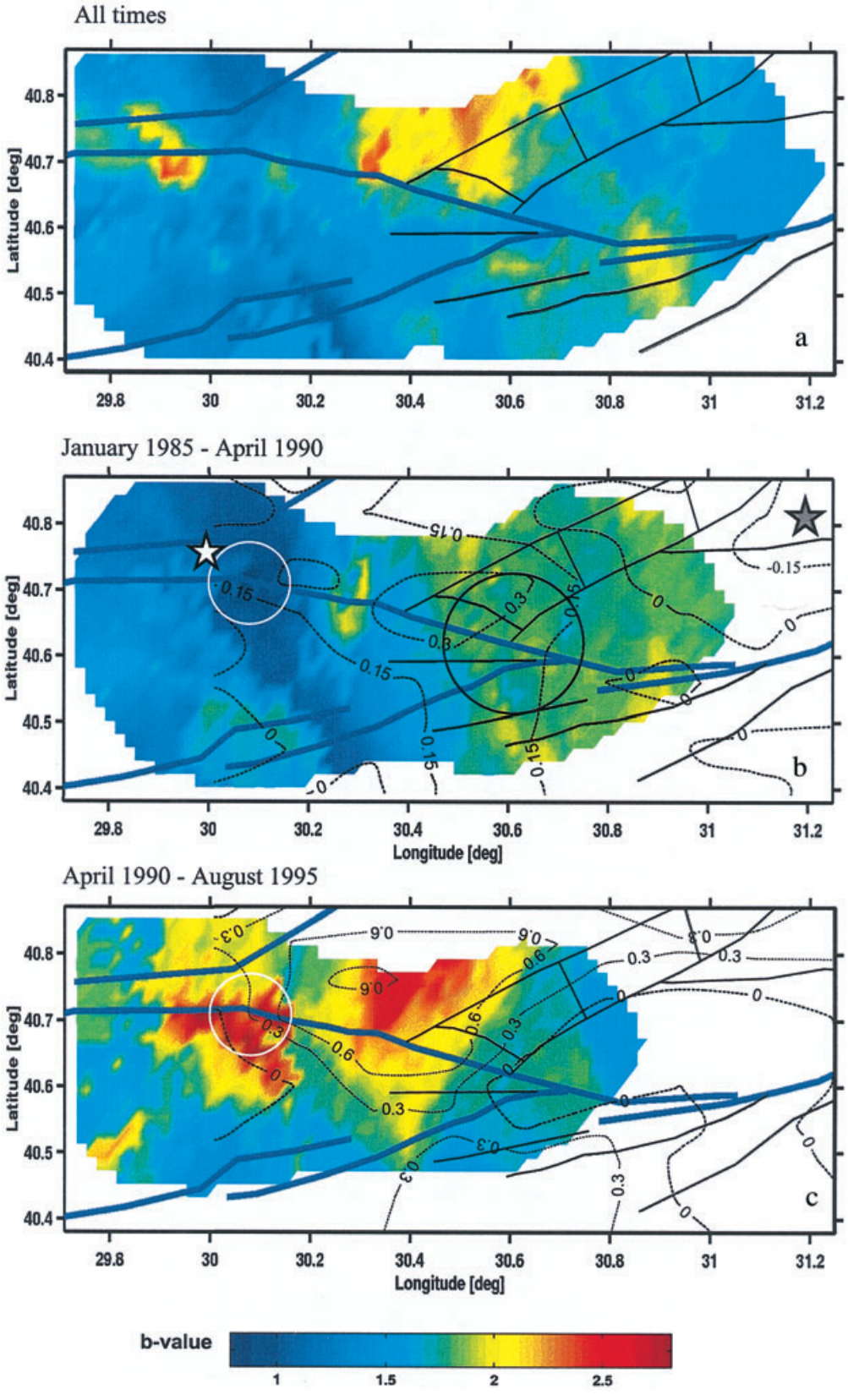

Figure 3. *b*-value maps for all earthquakes in the catalogue (a), and for two consecutive periods: January 1985 to April 1990 (b); and April 1990 to August 1995 (c). The number of earthquakes per sample is $n = 80$, the nodal separation is 0.02°, and the radius of the cylindrical sample volumes is $R \leq 25$ km. Along the seismically active fault segments west of 30.5°E, radii are typically less than 7 km. Circles indicate the crustal volumes used to check the significance of *b*-value differences in space and time (see Fig. 5). Dotted lines contour areal strain (in units of μstrain extension positive), as obtained from GPS observations between 1992 and 1995 (b) and 1991 and 1992 (c). Note the increased extension along the central and northwestern parts of the fault bend for the 1991–1992 campaigns. Stars mark the epicentres of the Izmit (white) and Düzce (grey) earthquakes.

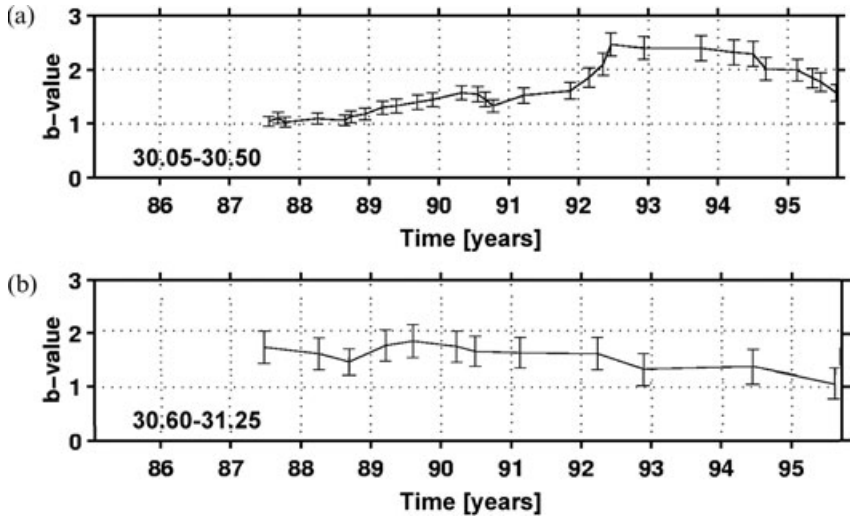

Figure 4. *b* value as a function of time in samples of 80, stepped at 16 events, with error bars for the areas bounded by longitudes (a) 30.05°E and 30.50°E, and (b) 30.60°E and 31.25°E.

In order to be sure that the contrasts of *b* can be accepted as reliable, we compare examples of FMDs in Fig. 5. The significance of the spatial variation is checked by comparing examples from the western margin and the centre of the fault bend at longitudes 30.1°E and 30.6°E, respectively. The circles in Fig. 3 indicate the locations as well as the extent of the areas sampled for the comparison. For the temporal variations, the location was fixed and examples were drawn from the pre-1990 and post-1990 data sets (white circles in Figs 3b and c). In both cases, the FMDs are judged to have probabilities of less than one per million of being drawn from the same population, based on Utsu's (1992) test, and their slopes also appear clearly different to the eye. Mean *b* values, calculated from the pre-1990 data for the regions west of 30.25°E (283 events) and east of 30.25°E (291 events), are 1.1 ± 0.1 and 1.7 ± 0.1, respectively. We summarize the observations as follows.

(1) The area investigated is separated into two *b*-value provinces. West of the fault bend normal values ($b_{mean} = 1.1 \pm 0.1$) prevail, while b_{mean} increases to 1.7 ± 0.1 within the bend. The increase is independent of depth. Farther to the east *b* may decrease again, but the seismicity is too low for this to be certain.

(2) In early 1992, *b* increases by an average of $+0.8$ in extended regions north of the fault junctions and along the

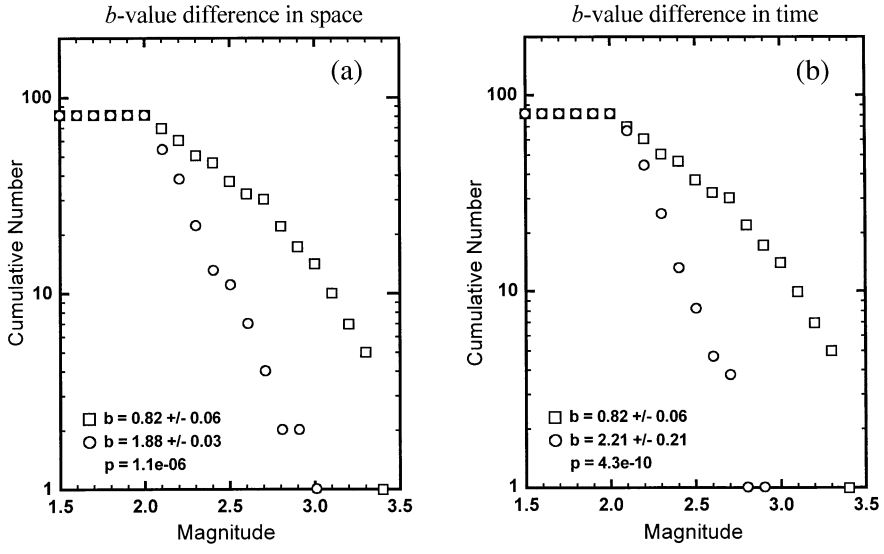

Figure 5. Comparisons of frequency–magnitude relations for various samples of earthquakes. (a) Fault segments near 30.1°E (squares) versus 30.6°E (circles). The volumes are indicated by white and black circles, respectively, in Fig. 3(b). (b) Fault segment near 30.1°E for two periods: 1985–1990 (squares) and 1990–1995 (circles), the volumes being indicated by white circles in Figs 3(b) and (c). The probability *p* that the compared samples come from the same population is shown in each frame.

western margin of the bend. The increase is most pronounced in the upper crust and is less clearly observed for earthquakes below a depth of 8 km.

(3) The spatial and temporal contrasts of *b* are statistically highly significant. The temporal variations in the central part of the area investigated are not caused by changes of the magnitude of completeness.

DISCUSSION

b value as a function of location

The relative spatial variations, by 54 per cent for the averages in the 'high' and 'low' provinces of *b* value, and by 130 per cent for selected subvolumes, are well within the range of variations observed along the strike of other fault zones (Wiemer & Wyss 1997; Wiemer & Benoit 1996) or earthquake ruptures (Wiemer & Katsumata 1999; Sobiesiak 2000). Thus, we accept the variations as reasonable and construct a physical model that could explain them.

Our interpretation of *b* as a function of location starts from the assumption that the spatial *b*-value distribution as shown in Fig. 3(b) is time-independent and reflects the normal background caused by the tectonic framework (the pattern does not change if we calculate *b* for the extended period of January 1985 to December 1991). Consequently, it is reasonable to assume that the enhanced *b* values east of 30.25°E are related to the fault bend and/or the fault junctions as the dominant structural features in this area. Areal extension in this region is expected due to the tensional sense of the bend and is corroborated by the geodetic data (Fig. 2). Since no GPS data are available prior to 1991, we take the interval 1992–1995 as being representative of the interseismic, tectonically induced deformation pattern. Under the premise that the tectonic stressing produces repeatable patterns, the isolines of deformation are plotted into the *b*-value map of the pre-1990 earthquake data (Fig. 3b). Regions of extension correlate reasonably well with regions of high *b* values. The correspondence is less conclusive at the edges of the map, where the density of either GPS stations (west of 30.1°E) or seismic events (east of 30.6°E) is too low. Other clues for an ongoing horizontal extension are fault plane solutions indicating considerable down slip and normal faulting simultaneously with abundant strike-slip. Thus, the two most important conditions for high *b* values, namely (1) low ambient stress and (2) strong material heterogeneity, presumably are fulfilled along the fault bend.

Accordingly, we interpret the increase of b_{mean} from 1.1 in the west to 1.7 within the fault bend to be due to the non-uniform stress field resulting in increased fracturing in a 3-D deformation field. The interference of horizontal and vertical tectonics presumably shortens the mean crack length. As a consequence of the low horizontal stresses, normal stress on the existing cracks is low; some fractures may even be kept open. Thus, microseismicity presumably is attributable to frictional sliding on existing cracks rather than to the propagation of new cracks. According to Scholz (1968), frictional sliding as the predominant mechanism for the radiation of seismic energy results in an enhancement ($b \geq 1.5$) and considerable stress dependence of *b* values. The important influence of normal stress on *b* has been confirmed by seismic observations indicating that high *b* values prevail in extensional tectonic regimes (Frohlich & Davis 1993), in crustal volumes at high pore pressure (Wyss 1973), and along creeping fault segments (Amelung & King 1997).

The lowest *b* values ($b \sim 0.8$) in the area investigated are found at the junction between the fault bend and the highly active, straight fault segment in the west. In a numerical approach, Nielsen & Knopoff (1998) showed that slip on the releasing segment induces localized zones of compression at the junctions between the bend and the adjacent straight fault segments. Thus, the *b*-value minimum at 40.7°N, 30.1°E presumably covers a site of stress concentration and high fracture strength. In our 1998 manuscript, we concluded: '*If the hypothesis that main shocks are more likely to emanate from fault segments with low b values (Wiemer & Wyss 1997) is correct, then the most likely location for a major earthquake along this section of the North-Anatolian fault is near 40.7°N/30.1°E. The fault segment running through this volume of low b values last ruptured in 1878. It was suggested by Toksöz et al. (1979) that this part of the fault system could be a potential seismic gap, since the westward migrating surface ruptures of the 1939–1967 earthquake sequence stopped at about 30.25°E. Stein et al. (1997) calculated the stress transferred by the most recent event of the sequence, the 1967 Mudurnu-Valley earthquake (M = 7.2), on the unbroken segments. They found that the western continuation of the fault, i.e. the segment with low b values, has been brought closer to failure by a change in Coulomb stress of 1.3–2.5 bars*' (quoted from Zschau 1998). According to Kandilli Observatory, the epicentre of the Izmit earthquake is located at 40.76°N, 29.97°E, about 13 km away from the anticipated site at 40.7°N, 30.1°E (Fig. 3b). The distance is even less than 10 km with respect to the epicentre coordinates given by USGS (40.702°N, 29.987°E). This close correspondence supports our interpretation of *b* as a tool to monitor the state of stress along a fault zone.

b value as a function of time

The hypothesis of a long-lasting asperity near 30.1°E is apparently put into question by the strong temporal *b*-value variations observed at this site. Changes in *b* value as a function of time can be due to changes in the reporting procedure by which the earthquake catalogue is compiled (e.g. Zuniga & Wyss 1995). In the data used here, there is no specific evidence that a reporting change took place at in early 1992. Furthermore, a correlation between the *b*-value variations and the improvement of the seismic network is not obvious. The fact that this change is observed only in the western part of the area monitored (Fig. 4) suggests that it is real rather than artificial. Nevertheless, we cannot rule out this possibility. To decide whether the temporal increase of *b* by ~ 70 per cent in areas north and west of the fault bend (180 per cent for the selected subvolume at 30.1°E, 40.7°N) can be accepted as real, we compare it with anomalous changes of other geophysical parameters.

Isolines of deformation indicate that the *b*-value anomaly coincides with intensified extension of the 'pull-apart' region of the fault bend (Fig. 3c). The areal extension obtained from the GPS campaigns in September 1991 and September 1992 reaches maximum values of up to 0.8 μstrain yr^{-1}, compared with 0.3 μstrain yr^{-1} for the period September 1992 to September 1995. Velocity differences between periods 1991–1992 and 1992–1995 are as high as 20 mm yr^{-1} for a cluster of three

GPS points along the northwestern part of the overstep (see Fig. 6a), but reduce to 7–11 mm yr^{-1} in the central and eastern parts of the area investigated. Averaged over the whole GPS network, the difference in the velocity amplitudes of the two time intervals is 11 ± 5 mm yr^{-1}. This general offset between pre-1992 and post-1992 GPS velocities is observed not only for the local Mudurnu network, but also for major GPS campaigns carried out in the Marmara region (Straub 1996; Straub *et al.* 1997) and in the whole of Anatolia (Reilinger *et al.* 1997). This velocity offset is probably an artefact caused by alterations in the data analysis routines (e.g. Straub 1996). As it is consistently observed across a 500 km × 800 km region throughout West and Central Anatolia, we assume that this apparent change in the velocity field is a large-scale effect that is homogeneous across our local 50 km × 130 km network. If this assumption holds, the much higher velocities of the cluster of GPS points between longitudes 30.4°E and 30.0°E, compared with the other points in the network, indicate a local transient effect. Anomalous strain rates between geodetic campaigns in 1991 and 1992 have also been observed within a 10 km × 10 km terrestrial network across a local tensional overstep at 31.0°E, 40.58°N (Franke *et al.* 1991; Westerhaus *et al.* 1997). Lühr *et al.* 1995) presented a list of various geophysical observation parameters along the southeastern fault segment that show rate changes in early 1992. Altogether, these observations strengthen the hypothesis that a transient local deformation phenomenon occurred in 1992. Taking into account the offset of 11 mm, the differential motion of the cluster reduces to about 9 mm. This is only slightly larger than the typical error of 6 mm. However, the fact that a cluster of points simultaneously show this increase raises our confidence in this anomaly.

Comparison of the differential velocity field and a differential *b*-value map shows a striking coincidence (Fig. 6). This differential *b*-value map was constructed using a single grid and subtracting the *b* value prior to 1990 from the value after that date. The *b* values increase significantly (95 per cent confidence) in the region in which an accelerated horizontal movement of a cluster of GPS monuments is observed. An opposite trend towards lower *b* values in the later period is observed within a narrow spot along the fault junction at 30.6E, 40.6 N. The decrease in *b* is compatible with local differential compression, as indicated by the relatively low velocities and the opposite components of motion of the two GPS stations in this area (see also Fig. 3). Although the temporal *b*-value anomaly presumably occurs in 1992, the two five-year intervals 1985–1990 and 1990–1995 are kept in order to have enough events for a reasonable spatial resolution.

A possible scenario

An increase in *b* value as a function of time is most reasonably explained by its inverse correlation to applied stress. However, we are not aware of any process that could have sufficiently changed the stress field in the area investigated during the past

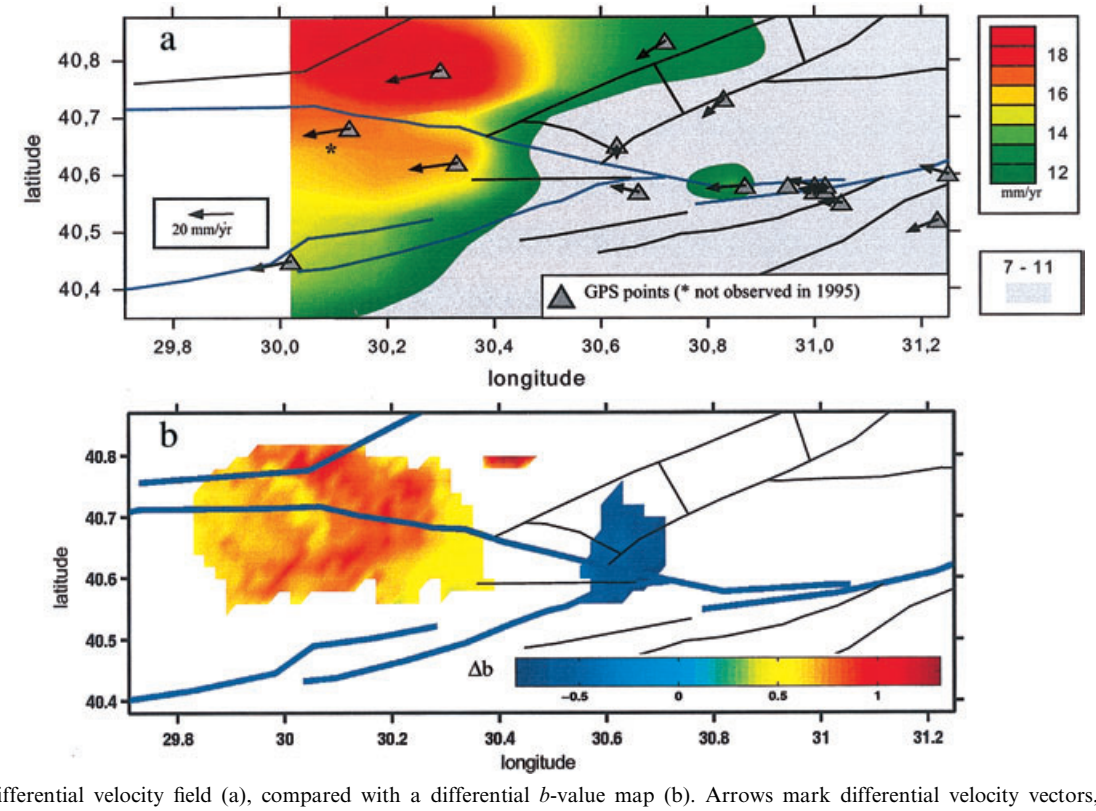

Figure 6. Differential velocity field (a), compared with a differential *b*-value map (b). Arrows mark differential velocity vectors, obtained by subtracting the averaged GPS campaigns 1992–1995 from the campaign 1991–1992. Colours indicate velocity amplitude differences smoothed over a 6 km by 14 km grid spanning the area of the 18 GPS sites, with higher velocities in 1991–1992. A general offset in the velocities of about 11 mm yr^{-1}, observed over the whole area investigated (grey colour), presumably is due to an inadvertent change in the GPS analysis routines. The *b*-value map has been derived by subtracting the pre-1990 from the post-1990 *b* values at each node of the same grid. A positive value (red colour) of Δb indicates higher *b* values in the later period. Nodes where changes are not statistically significant (95 per cent confidence) are not coloured. The radius of the sampling volumes is $R_{const} = 15$ km, and the number of earthquakes in each sample is $n \geq 50$.

10 years. The *b*-value increase in early 1992 coincides with two phases of swarm-like seismic activity (February 21–March 4 and March 24–March 31, 1992), clustering along the bending fault (Fig. 7). During these short active periods, 27 events with $2 \leq M \leq 3.2$ were located. The first cluster (30.39°E, 40.71°N) almost exactly matches the limited area where composite fault plane solutions indicate normal faulting with the fault plane dipping steeply towards the NE (Neugebauer *et al.* 1997; see also Fig. 2). Cluster 2 (30.61°E, 40.66°N) is located within a region of normal faulting with the extension axis striking NNW. Apart from these bursts of microseismic activity, the background rate decreased along the central and the eastern fault segments. West of 30.25°E, a two-year phase of reduced activity is followed by a considerable increase in the rate of seismic events.

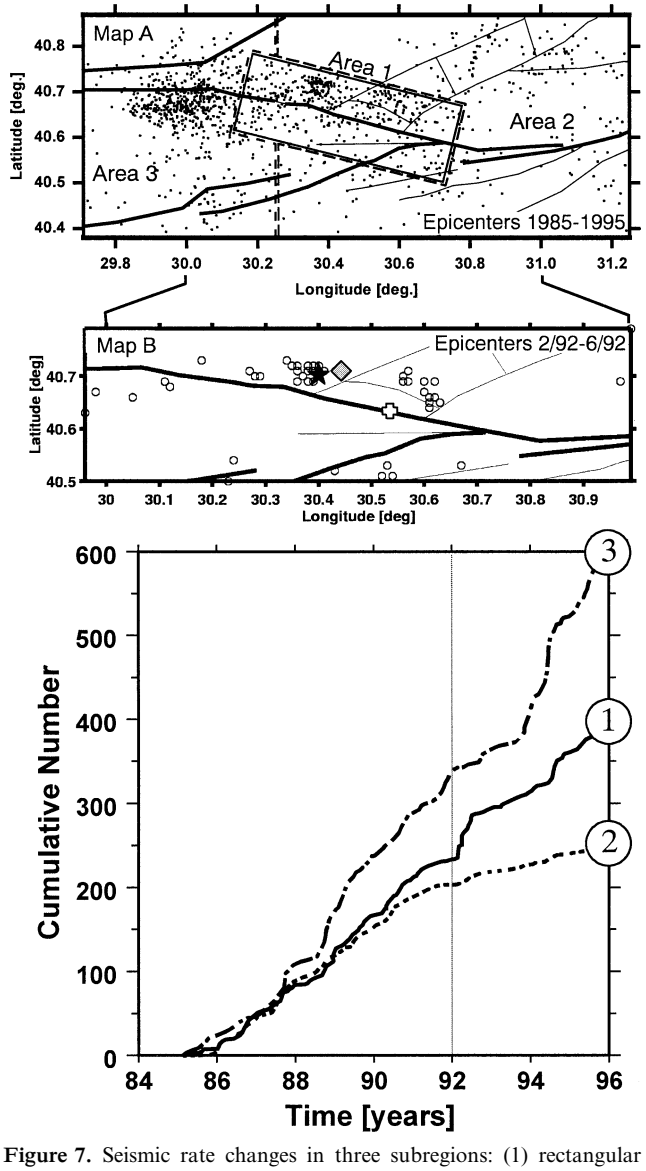

Figure 7. Seismic rate changes in three subregions: (1) rectangular area along the central part of the fault bend; (2) east of 30.25°E, excluding area (1); (3) west of 30.25°E, excluding area (1). The subregions are indicated in map A. The location of the swarm activity that is responsible for the steep increase in the cumulative number of earthquakes of area (1) in February/March 1992 is shown in map B. Large symbols indicate the epicentres of a $M_L = 5.6$ normal faulting earthquake on 1967 July 30 [Jackson & McKenzie 1984 (star); Dewey (1976) (cross)], and the slow event modelled in this study (diamond).

Although the number of swarm events during 18 days in February/March 1992 is equivalent to one year of the normal background rate, this activity is too small to account for the observed deformation changes. We therefore hypothesize that the swarm activity is a side-effect of one (or several) slow earthquakes with equivalent magnitudes much larger than those of the microearthquakes. Creep is generally associated with high *b* values (e.g. Amelung & King 1997). Phases of stable aseismic slip preceding unstable stick slip are known from laboratory experiments (e.g. Dietrich 1978) and have been confirmed for natural faults (e.g. Kanamori & Stewart 1979). With improved geodetic networks and seismological data analysis techniques, silent earthquakes and creep events have recently been documented that did not induce brittle rupture (e.g. Heki *et al.* 1997). Several creep episodes were accompanied by moderate seismic activity (e.g. Linde *et al.* 1996). Moreover, a section of the North Anatolian Fault near Ismet Pasa, about 180 km east of the Mudurnu Valley, is known to release stress by creep, as well as by earthquakes (Dewey 1976).

While the mechanism controlling the switching between seismic and aseismic energy release is not well understood at present, at least one condition favouring stable sliding—low normal stress—prevails along the fault bend in the centre of the area investigated. Thus, we hypothesize that local aseismic slip along the central fault segment might have caused the increase in *b* and the differential motion of the western GPS stations. We search for the simplest model capable of explaining the essential features of the observations. Okada's solutions for a dislocation in an elastic half-space (Okada 1992) are used to calculate surface displacement and stress changes at seismogenic depths. Various source models were tested with respect to the GPS data. The only simple model that reasonably explains the extensional character of the geodetic anomaly in 1992 is a normal faulting source with the extension axis striking WSW–ENE and the fault plane dipping towards the ENE. This mechanism is compatible with the style of deformation in this region (*cf.* Fig. 2). A strong aftershock of normal fault type ($M_L = 5.6$, T-axis orientated SE–NW), occurring 8 days after the 1967 July 22 catastrophic earthquake, indicates that this fault segment is capable of producing extensional events of considerable magnitude. According to Jackson & McKenzie (1984), the epicentre of this earthquake was located at 30.40°E, 40.70°N, adjacent to cluster no. 1 (Fig. 7). The depth was estimated as 16 km. Dewey (1976) placed the epicentre at 30.53°E, 40.63°N, a location between the two clusters, with the hypocentre restrained to a depth of 15 km.

A satisfactory model is shown in Fig. 8. The fault plane of the model has a length of 14 km and a width of 6 km; the strike is N10°W and the dip angle is 70° towards NNE. The midpoint of the plane is located at 30.43°E, 40.71°N at a depth of 10 km, close to the epicentre of the 1967 aftershock (Fig. 7). A slip of 0.3 m is assumed with the eastern block thrown down, resulting in an equivalent magnitude of the model event of $M_W = 5.9$. To calculate the stress, $\lambda = \mu = 33$ GPa are assumed for the Lamé parameters. Six GPS points are affected by the calculated surface displacements (Fig. 8a). The uniform differential movement of the cluster of the neighbouring points 2, 3, 4 is essentially explained. No significant EW-component of motion remains, after subtracting the suspected regional offsets

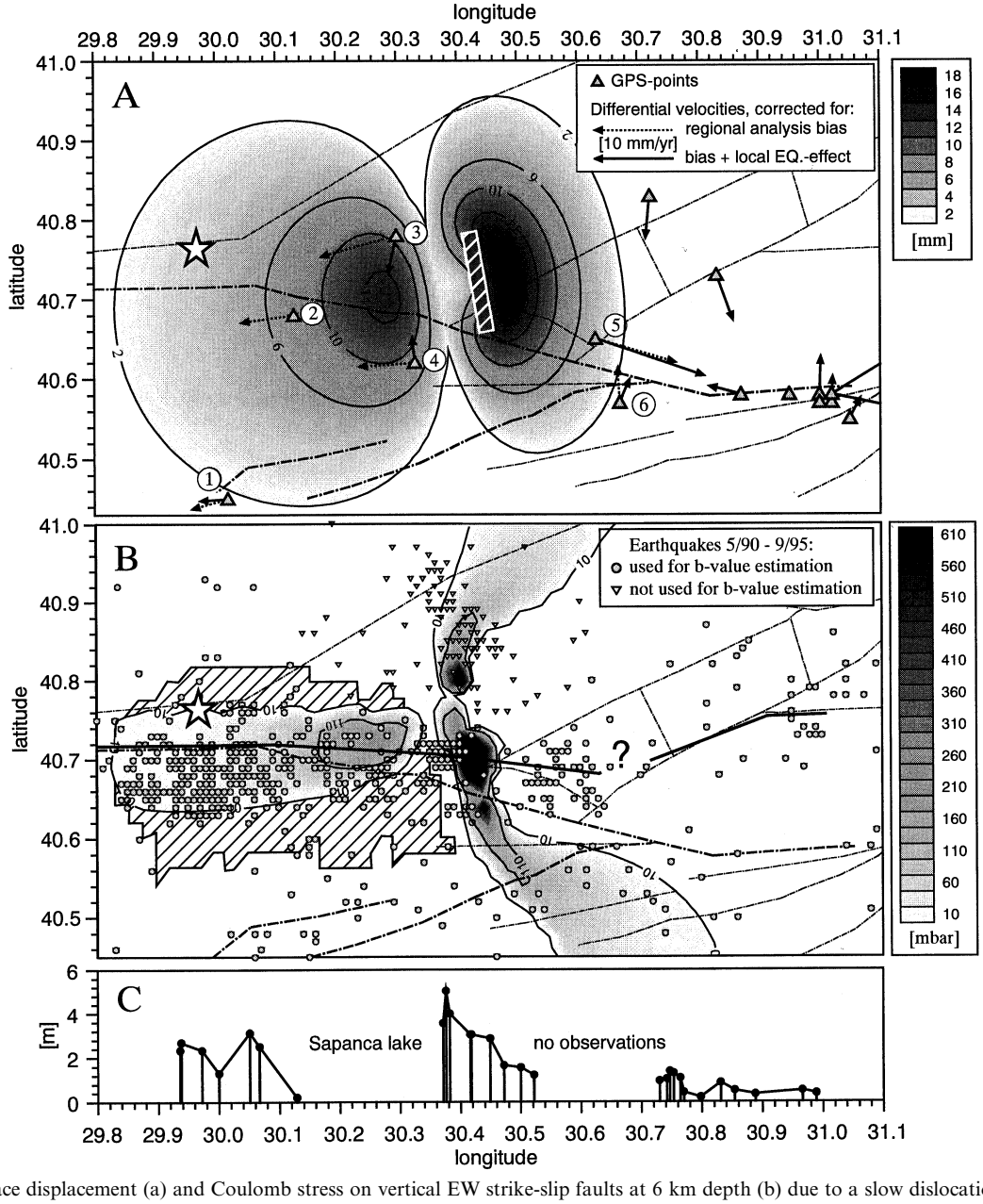

Figure 8. Surface displacement (a) and Coulomb stress on vertical EW strike-slip faults at 6 km depth (b) due to a slow dislocation at depth. The model assumes downward slip $d=0.3$ m on a fault plane of length $l=14$ km and width $w=6$ km, striking N10°W and dipping towards E by $\alpha=70°$. The midpoint of the fault plane is located at a depth of 10 km; white lines mark the projection of the fault to the surface. The equivalent magnitude is $M_W=5.9$. The star marks the epicentre of the Izmit earthquake. In (a) arrows illustrate the differential GPS velocities (before versus after 1992), after subtracting a suspected regional analysis bias of 9.8 mm yr^{-1} in an EW- and 2.4 mm yr^{-1} in a NS-direction (dotted arrows) and the local dislocation effect (straight arrows). In (b) the Coulomb stress has been resolved on vertical fault planes where the stress condition $\Delta\text{shear}\leq 0$ and $\Delta\text{Coulomb}\geq 0$ is fulfilled. The strike of the planes varies between N80°W and N100°W; for each direction of strike, the maximum Coulomb stress was plotted. The hatched area outlines the sites of significant *b*-value increase according to Fig. 6. The lower panel (c) shows surface displacements after the Izmit earthquake (source: German Seismological Task Force; personal communication H. Grosser & W. Welle 1999).

between campaigns 1992 and 1993/1995 (9.8 mm yr^{-1} in an EW- and 2.4 mm yr^{-1} in a NS-direction) and the displacements induced by the dislocation source. The residuals indicate a NS-contraction of the fault zone that is not discussed here. Fig. 9 shows a projection of the velocity amplitudes on the EW-direction as a function of longitude, disregarding the suspected regional offsets. By subtracting the displacements induced by the model event, the rate differences (for five out of the six affected points) are shifted towards the mean value; the standard deviation is reduced by 17 per cent. The model, however, fails for point no. 5.

The influence of the hypothesized creep event on the seismic rate and the *b*-value distribution depends on the orientation of the active fault segments with respect to the induced stress changes. The regional decrease of the seismicity rate indicates that no faults exist that are optimally oriented to a reduction of

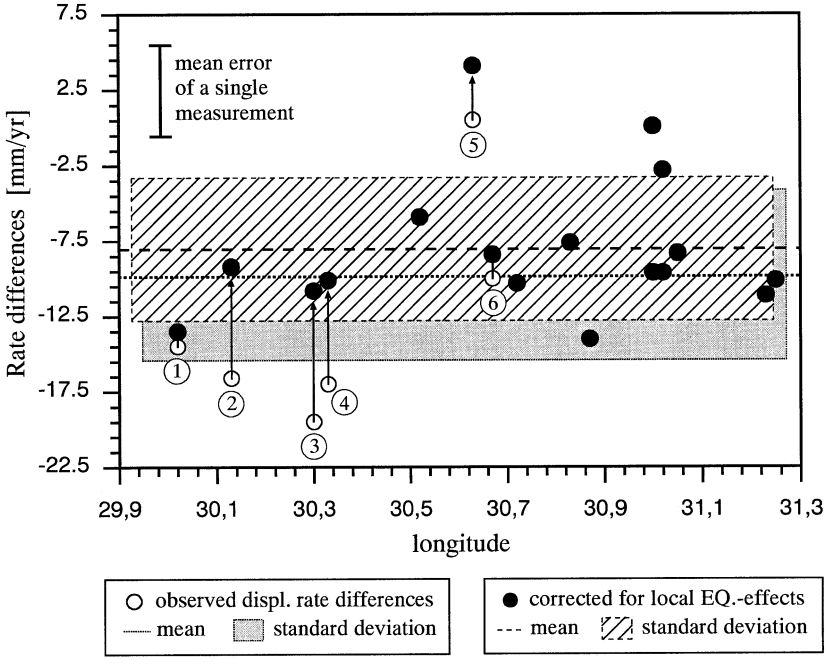

Figure 9. Changes of the differential velocity amplitudes due to the modelled silent earthquake. The locations of the numbered stations are shown in Fig. 8; white and black circles mark observed and corrected values, respectively. The differential velocity vectors have been projected on the EW-direction; negative values indicate westward movements.

effective stress. A local reduction of shear stress, moving the system away from failure, would explain a period of seismic quiescence. However, the contributions of that area to the ensemble of events used to determine the *b* value would be reduced simultaneously, and the information about a temporal change in *b* might be suppressed by including seismicity from neighbouring areas or by averaging over a long period. Thus, in our opinion, the most promising environments in which to detect an increase in *b* are those where shear as well as mean stress is reduced, while Coulomb stress remains constant or increases. In this case, the trigger potential is the same or higher than before, but the earthquakes now occur in a low-stress environment. Consequently, we look for fault segments where the condition: $\Delta\text{shear} \leq 0$ and $\Delta\text{Coulomb} \geq 0$ holds.

We restrict our investigations in our model to the predominating faulting mechanism north of the fault bend and along its western margin, where the largest *b*-value anomalies are found, and resolve the stresses on vertical strike-slip faults and dipping faults with the same strike as the model event. Coulomb stress, σ_f, is calculated at a depth of 6 km according to the formula

$$\sigma_f = \tau + \mu\sigma_n\,, \tag{3}$$

where τ is the shear stress (positive in the direction of fault slip), σ_n is the normal stress (compression negative), and μ is the apparent coefficient of friction. Stein *et al.* (1997) use $\mu = 0.4$ to account for pore pressure effects during changes of applied stress. There are some indications that, within the area investigated, pore pressure at depth is hydrostatic and any pore pressure variation is eradicated by diffusion within a few months. Therefore, we adopt a value $\mu = 0.75$, equivalent to laboratory values.

For the normal faulting mechanism of small background earthquakes proposed in our scenario, the condition $\Delta\text{shear} \leq 0$ and $\Delta\text{Coulomb} \geq 0$ is fulfilled only in a narrow, 20 km long patch above the fault plane of the creep event. Events of normal fault type triggered under these conditions may contribute to the anomaly north of the fault bend; however, *b* values in this region are generally high and the 1992 increase is not significant at a 95 per cent confidence level. A more complicated pattern evolves for strike-slip earthquakes (Fig. 8b). The stresses are resolved on vertical faults with variable strike in directions EW $\pm 10°$. For each direction of strike, the maximum Coulomb stress is plotted. Thus, shaded areas in Fig. 8(b) indicate regions where the trigger conditions for right-lateral strike-slip earthquakes on vertical faults with an orientation varying between N80°E and N100°E are improved, while shear and normal stresses on the faults are reduced. The stress criterion is fulfilled within three long club-like areas.

The first one extends along the western margin of the fault bend towards the west. It encompasses the majority of microearthquakes along these segments and coincides with the area of significant *b*-value increase in 1992. The spatial correlation is obvious; we conclude that normal faulting along the central part of the releasing bend during the opening of a pull-apart basin establishes the conditions for the triggering of strike-slip earthquakes under low stress and, hence, potentially promotes a *b*-value increase along the western fault segments. Simultaneously, the conditions for normal faulting along these segments become worse. The relative number of strike-slip versus normal faulting events presumably increases. The calculated stress changes are of the order of 100 mbar, which seems to be quite low. The stress values depend on the elastic moduli, hypocentre parameters of the responsible creep event, and potential distortions of the homogeneous deformation fields due to the presence of the faults, and could be increased with an appropriate choice of one or more of these quantities. On the other hand, a correlation between microseismic activity

and river discharge, observed in our area as well as at other places (e.g. Wolf *et al.* 1997), suggests that changes in effective stress even of less than 100 mbar might be sufficient to induce earthquakes if the crust is in a critical condition.

It is interesting to compare these results, which have been derived from pre-1999 data, with seismotectonic features of the Izmit earthquake of 1999 August. The surface rupture of the main shock crosses the overstep north of the southward-bending main fault (Fig. 8b). In this region, the rupture seems not to be associated with known fault traces, but follows the EW-striking zone of positive Coulomb stress change arising from the 1992 slow event that we propose, passing through the local and absolute maxima at 30.26°E (ΔCoulomb > 180 mbar) and 30.44°E (ΔCoulomb > 3 bar), respectively. The site of maximum positive Coulomb stress change, calculated on the basis of our model for a slow earthquake, matches the site of maximum observed surface displacement after the Izmit earthquake to within 5 km (Figs 8b and c). The observed surface offsets decrease continuously towards the central part of the fault bend and are also small along the northeastern branches (Fig. 8c). At these sites, Coulomb stress change due to the 1992 silent event is negative; that is, the east–west strike-slip faulting is inhibited. Within a radius of 20 km from the epicentre of the slow event, the reduction in stress along these segments is larger than the regional tectonic stress rate of ~ 150 mbar yr^{-1}. With a stress release equal to one year of tectonic loading, a perceptible collapse of microseismic activity as observed for the region east of 30.25°E (see Fig. 7) has to be expected. Thus, the proposed 1992 slow event, as well as any other earthquake of normal fault type accommodating the formation of a pull-apart basin in the northwestern part of the bend, unclamped the Izmit rupture plane west of 30.4°E but increased the resistance to slip on that plane east of 30.4°E. The clamping/unclamping mechanism might be a possible explanation for the strong local differences in surface displacement as observed after the Izmit earthquake (e.g. Perfettini *et al.* 1999).

The second beam of change seen in Fig. 8 coincides largely with a strip of enhanced seismicity that emanates from the fault bend near the junction and trends in a northerly direction. These events are known to exhibit a high *b* value, but are potentially contaminated by quarry blasts and are not used for this study.

The third beam trends towards the southeast. In this region, no significant increase in *b* is observed, and seismicity is generally lower as in the other regions. According to Neugebauer *et al.* 1997), normal faulting is the prevailing mechanism in this region, and it seems plausible to assume that the stress conditions are generally unfavourable for EW strike-slip faulting, or that appropriate fault planes do not exist. For normal fault planes with an orientation similar to the composite fault plane solution presented by Neugebauer *et al.* (1997), the stress condition for higher *b* values is not fulfilled, and thus significant changes in seismic activity or in *b* are not expected in this region.

CONCLUSIONS

We have shown that the *b* value changes significantly along a large-scale bend of the North Anatolian fault. High values ($b_{\mathrm{mean}} = 1.7$) are found within the bend and towards the northeast, while normal values ($b_{\mathrm{mean}} = 1.1$) prevail in the west. We conclude that the *b*-value high along the fault bend is favoured by a locally high degree of heterogeneity, which we propose comes about through extensive fracturing near the junction of the bending main fault trace and a subparallel-striking fault system. We suggest that the potential effect of the complex crack field on *b* value is enhanced by low horizontal stresses. Normal faulting, areal extension as obtained from GPS measurements, and geological evidence for subsidence in that region are compatible with the concept of an opening pull-apart basin. Owing to low normal stress, slip on pre-existing cracks predominates over the propagation of new cracks, resulting in high *b* values.

Since there is a plausible explanation for the *b*-value increase east of 30.25°E, we conclude that the *b*-value minimum at 40.7°N, 30.1°E also has a physical meaning. At this location, calculation of tectonic strain is not possible, because the GPS network does not extend into that area. However, a stress concentration at the junction between straight and bending fault segments is expected from numerical models of seismicity along geometrical barriers. In Zschau (1998), we thus concluded that the *b*-value minimum might indicate the most likely place for a future earthquake in the region. The conclusion was confirmed by the Izmit earthquake of 1999 August 17. The earthquake nucleated along, or slightly north of, the straight fault segment connected to the overstep, 10 to 13 km west of the site anticipated by the *b*-value evaluation.

An increase in *b* by an average of $+0.8$ in early 1992 coincides with a period of intensified extension over a sediment-filled depression north of the fault bend and pronounced swarm activity. We assume that the swarm activity and the apparent extension indicate a phase of intensive folding in accordance with the opening of a pull-apart basin. To test this hypothesis, we calculated the changes in displacement and stress due to a dislocation at depth. It was found that the differential movements of five GPS points are reasonably well explained by a downward slip on a fault plane striking N10°W and dipping 70° towards ENE. The equivalent magnitude of the hypothesized slow event is $M_{\mathrm{W}} = 5.9$. Since no main shock was recorded, we hypothesize that the faulting process could be slow. The effect of the event on the *b*-value distribution was tested under the assumption that *b* is most likely to increase in regions where both deviatoric and mean stress are diminished, while Coulomb stress is not reduced. At a depth of 6 km, this stress condition is fulfilled for earthquakes of strike-slip type along the western margin of the bend and the adjoining fault segment, coinciding well with the regions of strongest *b*-value increase. We thus conclude that the model event is capable of inducing the observed *b*-value changes, if EW strike-slip is the predominant faulting mechanism in these areas. The Coulomb stress changes lowered the resistance to slip on the western and central parts of the rupture plane of the 1999 Izmit earthquake, which was of right-lateral strike-slip type. Sites of peak stress change coincide with sites of peak surface slip. Thus, the 1992 slow event, like any other earthquake of normal fault type in that region, would have unclamped the 1999 Izmit fault, and, in *sensu latu*, can be considered as a foreshock of the Izmit $M_{\mathrm{W}} = 7.4$ earthquake.

The assumption of a dislocation source in a homogeneous half-space and a dip-slip mechanism without any strike-slip component is probably an oversimplification of the complex situation along the fault bend. Despite its simplicity, however, the scenario provides a plausible and conclusive explanation for the observed temporal changes. We are aware that some of our conclusions are somewhat speculative. Serious arguments against our scenario are: (1) the calculated stresses seem to

be quite low compared with the magnitude of the temporal variations; (2) the apparent changes in the GPS data are not significant according to a 95 per cent confidence criterion; (3) we cannot be absolutely certain that the decrease in seismicity rate and the increase in *b* are not due to changes in the reporting procedure of events in the earthquake catalogue; and (4) seismic and geodetic data do not cover exactly the same area nor the same periods of time.

In the face of these weaknesses, we hesitate to talk about a 'model'; rather, we would like to call our considerations a plausible scenario. The most important next step is to extend the seismic and geodetic time series and to incorporate further, independent data sets into the calculations. For several years, a general change in the state of deformation in early 1992 has been discussed by workers in this area as the cause for trend changes in various parameters of the interdisciplinary observation network along the southeastern margin of the fault bend. Our scenario is the first quantitative realization of this idea. The significance of the general assumption that the observed temporal variations reflect real changes in the state of deformation along the NAF increases strongly by a combination of the results of different, independent experiments.

We conclude that *b*-value mapping can unlock relevant information about the condition of the crust near active faults, and that comparison of changes in *b* with changes of other geophysical parameters may lead to an understanding of what these *b*-value changes mean. Once such an understanding is reached, one may be able to map indirectly the state of stress and of heterogeneity in seismically active areas.

ACKNOWLEDGMENTS

This paper is a contribution to the joint German–Turkish Project on Earthquake Research. We thank H. Berckhemer and B. Baier (Institute of Meteorology and Geophysics, Frankfurt University, Germany) and A. Yatman (Earthquake Research Institute, Ankara, Turkey) for preparing and providing the earthquake catalogue of the years 1985–1995. The GPS measurements were performed and processed by the Institute for Applied Geodesy, Frankfurt (now Bundesamt fuer Kartographie und Geodaesie) in cooperation with the Istanbul Technical University and the General Command of Mapping, Ankara, under the direction of H. Seeger, A. Aksoy, P. Franke and Y. Altiner. We are grateful to S. Wiemer for making available new subroutines for ZMAP quickly via the Internet, and to F. Roth for poviding a computer code for Okada's solutions. We thank G. W. Michel, B.-G. Lühr, H. Woith, C. Milkereit, G. Bock and two anonymous readers for critical comments and valuable suggestions on the manuscript, and R. Stromeyer for preparing GMT-graphs (Wessel & Smith 1991). The research was funded by the German Research Foundation (Project Zs 4/4), the GeoForschungsZentrum Potsdam, and the AFET General Directorate of Disaster Affairs. One of us (MWy) was supported by the NSF, grant number EAR-9902717, as well as the Wadati Foundation at the Geophysical Institute, University of Alaska, Fairbanks, during a one year stay at GFZ Potsdam.

REFERENCES

Altiner, Y., 1996. Geometrische Modellierung Innerer und Äußerer Deformationen der Erdoberfläche, *PhD thesis,* Institute für Angewandte Geodäsie, Heft no. 462, Frankfurt.

Amelung, F. & King, G., 1997. Earthquake scaling laws for creeping and non-creeping faults, *Geophys. Res. Lett.,* **24,** 507–510.

Barka, A.A., 1992. The North-Anatolian Fault Zone, *Annales Tectonicae, Firenze, Italy,* **6** (Suppl.), 164–195.

Barka, A.A. & Kadinsky-Cade, K., 1988. Strike-slip fault geometry in Turkey and its influence on earthquake activity, *Tectonics,* **7,** 663–684.

Bender, B., 1983. Maximum likelihood estimation of b-values for magnitude grouped data, *Bull. seism. Soc. Am.,* **73,** 831–851.

Dewey, J.W., 1976. Seismicity of Northern Anatolia, *Bull. seism. Soc. Am.,* **66,** 843–868.

Dietrich, J.H., 1978. Preseismic fault slip and earthquake prediction, *J. geophys. Res.,* **86,** 3940–3948.

Ergünay, O. & Zschau, J., 1989. Introduction to the Turkish-German Earthquake Research Project, in *Turkish-German Research Project, Report 25th Assem. IASPEI,* pp. 1–17, eds Zschau, J. & Ergünay, O., Geophysical Institute, University of Kiel, Kiel.

Franke, P., Altiner, Y. & Deniz, R., 1991. Messungen mit dem MEKOMETER ME-5000 im Rahmen der 'Geodätisch-geophysikalischen Untersuchungen entlang der Nordanato-lischen Störzone', *Vermessungswesen Raumordnung,* **53,** 65–77 (in German).

Frohlich, C. & Davis, S., 1993. Teleseismic b-values: or, much ado about 1.0, *J. geophys. Res.,* **98,** 631–644.

Gutenberg, R. & Richter, C.F., 1944. Frequency of earthquakes in California, *Bull. seism. Soc. Am.,* **34,** 185–188.

Heki, K., Miyazaki, S. & Tsuji, H., 1997. Silent fault slip following an interplate thrust earthquake at the Japan Trench, *Nature,* **386,** 595–597.

Ishimoto, M. & Iida, K., 1939. Observations of earthquakes registered with the microseismograph constructed recently, *Bull. Earthq. Res. Inst.,* **17,** 443–478.

Jackson, J. & McKenzie, D., 1984. Active tectonics of the Alpine-Himalayan Belt between western Turkey and Pakistan, *Geophys. J. R. astr. Soc.,* **77,** 185–264.

Kanamori, H. & Stewart, G.S., 1979. A slow earthquake, *Phys. Earth. planet. Inter.,* **11,** 167–175.

Linde, A.T., Gladwin, M.T., Johnston, M.J.S., Gwyther, R.L. & Bilham, R.G., 1996. A slow earthquake sequence on the San Andreas fault, *Nature,* **383,** 65–68.

Lopez Casado, C., Sanz de Galdeano, C., Delgado, J. & Peinado, M.A., 1995. The b parameter in the Betic Cordillera, Rif and nearby sectors. Relations with the tectonics of the region, *Tectonophysics,* **248,** 277–292.

Lühr, B.-G., Westerhaus, M., Woith, H. & Yatman, A., 1995. Temporal changes in various geoparameters accompanying seismic quiescence along a western part of the North-Anatolian Fault, *Terra Abstracts,* **7** (Suppl. 1 to TERRA Nova), 174.

McKenzie, D.P., 1972. Active tectonics of the Mediterranean region, *Geophys. J. R. astr. Soc.,* **30,** 109–185.

Main, I.G., 1991. A modified Griffith criterion for the evolution of damage with a fractal distribution of crack lengths: application to seismic event rates and *b*-values, *Geophys. J. Int.,* **107,** 335–362.

Main, I.G., Meredith, P.G. & Sammonds, P.R., 1992. Temporal variations in seismic event rate and *b*-values from stress corrosion constitutive laws, *Tectonophysics,* **211,** 233–246.

Meredith, P.G., Main, I.G. & Jones, C., 1990. Temporal variations in seismicity during quasi-static and dynamic rock failure, *Tectonophysics,* **175,** 249–268.

Michel, G., 1994. Neo-kinematics along the North-Anatolian Fault (Turkey), *PhD thesis,* Tübinger geowiss. Arb., Reihe A 16.

Mogi, K., 1962. Magnitude-frequency relation for elastic shocks accompanying fractures of various materials and some related problems in earthquakes, *Bull. Earthq. Res. Inst,* **40,** 831–853.

Neugebauer, J., Löffler, M., Berckhemer, H. & Yatman, A., 1997. Seismic observations at an overstep of the western North-Anatolian Fault (Abant-Sapanca region, Turkey), *Geol. Rund.,* **86,** 93–102.

Nielsen, S.B. & Knopoff, L., 1998. The equivalent strength of geometrical barriers to earthquakes, *J. geophys. Res.,* **103,** 9953–9965.

Okada, Y., 1992. Internal deformation due to shear and tensile faults in a half space, *Bull. seism. Soc. Am.,* **82,** 1018–1040.

Öncel, A.O., Main, I.G., Alptekin, Ö. & Cowie, P., 1996a. Temporal variations in the fractal properties of seismicity in the North Anatolian Fault Zone between 31°E and 41°E, *Pure appl. Geophys.,* **146,** 147–159.

Öncel, A.O., Main, I.G., Alptekin, Ö. & Cowie, P., 1996b. Spatial variations of the fractal properties of seismicity in the Anatolian fault zones, *Tectonophysics,* **257,** 189–202.

Perfettini, H., Stein, R.S., Simpson, R. & Cocco, M., 1999. Stress transfer by the 1988–89 M = 5.3 and 5.4 Lake Elsman foreshocks to the Loma Prieta fault: unclamping the site of peak mainshock slip, *J. geophys. Res.,* **104,** 20 169–20 182.

Reilinger, R.E., McClusky, S.C., Oral, M.B., King, R.W., Toksöz, M.N., Barka, A.A., Kinik, I., Lenk, O. & Sanli, I., 1997. Global Positioning System measurements of present-day crustal movements in the Arabia-Africa-Eurasia plate collision zone, *J. geophys. Res.,* **102** (B5), 9983–9999.

Scholz, C.H., 1968. The frequency-magnitude relation of microfracturing in rock and its relation to earthquakes, *Bull. seism. Soc. Am.,* **58,** 399–415.

Shi, Y. & Bolt, B.A., 1982. The standard error of the magnitude-frequency b-value, *Bull. seism. Soc. Am.,* **72,** 1677–1687.

Sobiesiak, M., 2000. Fault plane structure of the Antofagasta, Chile, earthquake of 1995, *Geophys. Res. Lett.,* **27,** 577–600.

Stein, R.S., Barka, A.A. & Dieterich, J.H., 1997. Progressive failure on the North-Anatolian fault since 1939 by earthquake stress triggering, *Geophys. J. Int.,* **128,** 594–604.

Straub, C., 1996. Recent crustal deformation and strain accumulation in the Marmara Sea region, N.W. Anatolia, inferred from GPS measurements, *PhD thesis,* Swiss Federal Institute of Technology, Zurich.

Straub, C., Kahle, H.G. & Schindler, C., 1997. GPS and geologic estimates of the tectonic activity in the Marmara Sea region, NW Anatolia, *J. geophys. Res.,* **102,** 27 587–27 601.

Tibi, R., Bock, G., Xia, Y., Baumbach, M., Grosser, H., Milkereit, C., Karakisa, S., Zünbül, S., Kind, R. & Zschau, J., 2001. Rupture process of the 1999 August 17 Izmit and November 12 Düzce (Turkey) earthquakes, *Geophys. J. Int.,* **144,** F1–F7.

Toksöz, M.N., Shakal, A.F. & Michael, A.J., 1979. Space-time migration of earthquakes along the North-Anatolian Fault Zone and seismic gaps, *Pure appl. Geophys.,* **117,** 1258–1270.

Tse, S.T. & Rice, J.R., 1986. Crustal earthquake instability in relation to the depth variation of frictional slip properties, *J. geophys. Res.,* **91,** 9452–9472.

Urbancic, T.I., Trifu, C.I., Long, J.M. & Toung, R.P., 1992. Space-time correlations of b-values with stress release, *Pure appl. Geophys.,* **139,** 449–462.

Utsu, T., 1992. On seismicity, in *Report of the Joint Research Institute for Statistical Mathematics,* **Vol. 34**, pp. 139–157, Institute for Statistical Mathematics, Tokyo.

Wessel, P. & Smith, W.H.F., 1991. Free software helps map and display data, *EOS, Trans. Am. geophys. Un.,* **72,** 445–446.

Westerhaus, M., Woith, H., Michel, G. & Franke, P., 1997. Pore pressure induced strain anomalies, *EOS, Trans. Am. geophys. Un.,* **78** (Fall Mtg Suppl), 158.

Wiemer, S., 1996. *ZMAP Users Guide,* Version 3.0, Geophysical Institute, University of Alaska, Fairbanks.

Wiemer, S. & Benoit, J., 1996. Mapping the b-value anomaly at 100 km depth in the Alaska and New Zealand subduction zones, *Geophys. Res. Lett.,* **23,** 1557–1560.

Wiemer, S. & Katsumata, K., 1999. Spatial variability of seismicity parameters in aftershock zones, *J. geophys. Res.,* **104,** 13 135–13 151.

Wiemer, S. & McNutt, S.R., 1997. Variations in the frequency-magnitude distribution with depth in two volcanic areas: Mount St. Helens, Washington, and Mount Spurr, Alaska, *Geophys. Res. Lett.,* **24,** 189–192.

Wiemer, S. & Wyss, M., 1997. Mapping the frequency-magnitude distribution in asperities: an improved technique to calculate recurrence times?, *J. geophys. Res.,* **102** (B7), 15 115–15 128.

Wiemer, S., McNutt, S.R. & Wyss, M., 1998. Temporal and three-dimensional spatial analysis of the frequency-magnitude distribution near Long Valley Caldera, *Geophys. J. Int.,* **134,** 409–421.

Wolf, L.W., Rowe, C.A. & Horner, R.B., 1997. Periodic seismicity near Mt. Ogden on the Alaska-British Columbia Border: a case for hydrologically triggered earthquakes? *Bull. seism. Soc. Am.,* **87,** 1473–1483.

Wyss, M., 1973. Towards a physical understanding of the earthquake frequency distribution, *Geophys. J. R. astr. Soc.,* **31,** 341–359.

Wyss, M., Westerhaus, M., Berckhemer, H. & Ates, R., 1995. Precursory seismic quiescence in the Mudurnu Valley, North-Anatolain Fault Zone, Turkey, *Geophys. J. Int.,* **123,** 117–124.

Wyss, M., Shimazaki, K. & Wiemer, S., 1997. Mapping active magma chambers by b-values, *J. geophys. Res.,* **102,** 20 413–20 422.

Zschau, J., 1998. *Geodetic and Geophysical Investigations Along the Seismo-Active Part of the North-Anatolian Fault Zone,* Final report to the German Research Foundation.

Zuniga, R. & Wyss, M., 1995. Inadvertent changes in magnitude reported in earthquake catalogs: Influence on b-value estimates, *Bull. seism. Soc. Am.,* **85,** 1858–1866.